Trapping effects in wave-packet scattering in a double-quantum-dot Aharonov-Bohm interferometer

Roberto Romo,[1,*] Jorge Villavicencio,[1] and M. L. Ladrón de Guevara[2]

[1]*Facultad de Ciencias, Universidad Autónoma de Baja California, Apartado Postal 1880,22800 Ensenada, Baja California, México*

[2]*Departamento de Física, Universidad Católica del Norte, Casilla 1280, Antofagasta, Chile*

(Received 10 March 2012; revised manuscript received 5 July 2012; published 23 August 2012)

An exact analytical solution for the time evolution of cutoff Gaussian wave packets scattered by a double-quantum-dot Aharonov-Bohm interferometer is derived to analyze the trapping effects of the molecular states of the system. Our analysis reveals that the formation and decay of a quasistationary state at the Fano resonance produces a monochromatic emission embedded in the transmitted packet, characterized by a dominant frequency $\Omega_{av} = \varepsilon_n/\hbar$ with a finite time duration, where ε_n is the Fano resonance energy. We demonstrate that the duration of this coherent emission can be extended by narrowing the Fano resonance with appropriate variations of the Aharonov-Bohm phase. This emission is switched off in the limit of zero width, where the localization of the associated molecular state occurs.

DOI: 10.1103/PhysRevB.86.085447 PACS number(s): 73.21.La, 85.35.−p, 73.23.Hk

I. INTRODUCTION

The stationary properties of the electron transport in artificial molecules formed by special arrangements of quantum dots (QDs) has been the subject of intense research in the last years.[1–6] Special attention has been paid recently on the study of the dynamical aspects of the electron transport in these kind of systems, such as the effects of time-dependent perturbations[7] and analysis of transient phenomena.[8] A distinctive feature of these structures is the retention of the quantum phase coherence,[9,10] where the Fano effect is one of the most remarkable evidences.[11] A system that has attracted much attention for the richness and variety of the exhibited phenomena is the double-QD molecule embedded in an Aharonov-Bohm (AB) interferometer.[2–5,12] The existence of two different pathways for the electron transport allows the features of bonding and antibonding states of the molecule to manifest themselves in the conductance as Breit-Wigner and Fano resonances,[2,6] as well as in an asymmetrical density of states (DOS) characterized by two peaks of different heights and widths.[3,6] In these time-independent studies it has been established that there is a correspondence between the sharpest (widest) peak in the DOS and the Fano (Breit-Wigner) line of the conductance, where the narrowing of the sharpest DOS peak was interpreted as an increase of the lifetime of the corresponding molecular state. The aim of this work is to investigate, from a dynamical point of view, the effects of the formation and decay of this long-lived quasistationary state on the transient behavior of scattered Gaussian wave packets. The use of Gaussian wave packets has been a valuable tool to explore the effects of the transmission profile on the time evolution of scattering in systems whose resonance spectrum involves Fano resonances.[13,14] Here we use the approach based on cutoff Gaussian wave packets introduced in Ref. 15 to explore the behavior of the wave packet scattered by the double-QD structure in an AB interferometer. We perform a time-frequency analysis on the exact analytical solution for the transmitted wave packet, establishing a close link between its transient structure and the parameters of the two molecular resonances.

The paper is organized as follows. In Sec. II we present a description of the solution of the problem, which involves an exact analytical time-dependent solution of Schrödinger's equation for cutoff Gaussian wave packets in a quantum shutter setup. This approach takes into account explicit formulas of the transmission amplitude of the double-dot AB interferometer derived from the equation of motion method for the Green's function. Section III presents the main results, where we analyze the dynamics of the transmitted pulses, particularly the trapping effects of the Fano resonance of the system in the time evolution of scattered wave packets. Finally, in Sec. IV we present the concluding remarks.

II. MODEL

We first describe the quantum shutter approach used in tunneling of Gaussian wave packets across a resonant structure. This method allows us to obtain analytical solutions of the time-dependent Schrödinger equation at the transmitted side of the system, provided that the transmission amplitude $t(k)$ of the problem is known.[15] This approach deals with an incident cutoff wave packet $\psi(x,t=0) = A\, e^{-(x-x_0)^2/4\sigma^2} e^{ik_0 x}\Theta(-x)$ of effective width σ and incidence energy $E_0 = \hbar^2 k_0^2/2m$ and initially centered at a position $x = x_0$, impinging on the left edge of the resonant structure at $t = 0$, where A is the corresponding normalization constant. The time-dependent solution along the transmission region is given by[15]

$$\psi(x,t) = \frac{1}{(2\pi)^{3/4}}\sqrt{\frac{\sigma}{w(iz_0)}}\int_{-\infty}^{\infty} dk\, w(iz)\, t(k)\, e^{i\phi(k)}, \quad (1)$$

where $\phi(k) = kx - \hbar k^2 t/2m$ and $t(k)$ is the transmission amplitude of the problem. The $w(z)$ function in Eq. (1) is the known *complex error function*,[16] with arguments $z_0 = (x_0/\sqrt{2}\sigma)$, and $z = (x_0/2\sigma) + i(k_0 - k)\sigma$. In the small truncation regime, that is, when $|x_0/2\sigma| \gg 1$, $w(iz) \simeq 2e^{z^2}$, which, introduced in Eq. (1), gives

$$\psi(x,t) = \sqrt{\frac{\sigma}{\pi\sqrt{2\pi}}}\int_{-\infty}^{\infty} dk\, \mathcal{T}(k)\, e^{i[\phi(k)-(k-k_0)x_0]}, \quad (2)$$

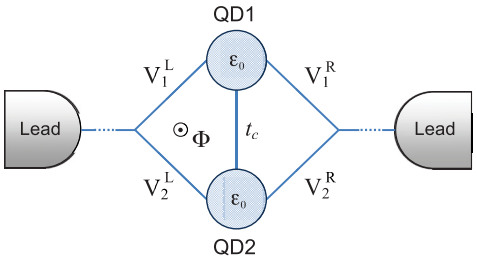

FIG. 1. (Color online) Double-QD AB interferometer where the tunnel matrix elements in the presence of a magnetic flux Φ are represented by $V_i^{L(R)}$ $(i = 1,2)$ and t_c is the interdot tunneling coupling. Just one energy level is assumed relevant in each of the dots, their energies being ε_0.

where $\mathcal{T}(k) \equiv t(k)e^{-(k-k_0)^2\sigma^2}$. The relevant input for Eq. (2) is the transmission amplitude $t(k)$ of the system in the momentum k space.

The resonant structure under consideration is a double-QD molecule embedded in an AB interferometer, the scheme of which is shown in Fig. 1. Only one level of energy ε_0 is assumed to be relevant in each of the QDs, the constant t_c is the tunnel coupling strength between dots, and $V_i^{L(R)}$ $(i = 1,2)$ is the coupling between the ith dot and the left (right) lead. A net magnetic flux Φ is enclosed by the interferometer. The system is modeled by a noninteracting Anderson Hamiltonian, which is given, for instance, in Ref. 2. The transmission amplitude $t(\varepsilon)$ can be obtained by the equation of motion method for the Green's function.[2,6] In the basis which diagonalizes the molecule Hamiltonian, the retarded Green's function $\mathbf{G}^r$ is given by

$$\mathbf{G}^r = \frac{1}{\Lambda}\begin{pmatrix} \varepsilon - \tilde{\varepsilon}_1 + i\tilde{\Gamma}_1 & 0 \\ 0 & \varepsilon - \tilde{\varepsilon}_2 + i\tilde{\Gamma}_2 \end{pmatrix}, \tag{3}$$

where $\tilde{\varepsilon}_1 = \varepsilon_0 - t_c$ and $\tilde{\varepsilon}_2 = \varepsilon_0 + t_c$ are the energies of the bonding and antibonding states, respectively, and

$$\tilde{\Gamma}_1 = 2\Gamma\cos^2(\phi/4) \quad \text{and} \quad \tilde{\Gamma}_2 = 2\Gamma\sin^2(\phi/4) \tag{4}$$

are their corresponding widths, where $\Gamma = 2\pi|V|^2\rho$, ρ being the DOS in the leads at the Fermi level. The constant Λ is defined as $\Lambda = (\varepsilon - \tilde{\varepsilon}_1 + i\tilde{\Gamma}_1)(\varepsilon - \tilde{\varepsilon}_2 + i\tilde{\Gamma}_2)$. The transmission amplitude can be deduced from the electron retarded Green's function from the relation[17]

$$t(\varepsilon) = \sum_{n,m} \bar{V}_i^R G^r_{n,m}(\varepsilon)\bar{V}_m^{L*}, \tag{5}$$

where $\bar{V}_n^{L(R)} = [2\rho_{L(R)}]^{1/2}\tilde{V}_n^{L(R)}$, with $\tilde{V}_n^{L(R)}$ the coupling matrix elements between the nth molecular state and the left (right) lead and $\rho_{L(R)}$ the DOS in the left (right) lead at the Fermi energy. Those matrix elements are

$$\tilde{V}_1^{L,R} = \frac{1}{\sqrt{2}}(V_1^{L,R} + V_2^{L,R}), \tag{6a}$$

$$\tilde{V}_2^{L,R} = \frac{1}{\sqrt{2}}(V_1^{L,R} - V_2^{L,R}), \tag{6b}$$

where $V_{1,2}^{L,R} = V_{1,2}^{L,R}(\phi)$ are given by $V_1^L = Ve^{i\phi/4}$, $V_1^R = Ve^{-i\phi/4}$, $V_2^L = Ve^{-i\phi/4}$, and $V_2^R = Ve^{i\phi/4}$, with $\phi = 2\pi\Phi/\Phi_0$, the AB phase, where $\Phi_0 = h/e$ is the flux quantum.

Evaluating Eq. (5) we obtain

$$t(\varepsilon) = \frac{\tilde{\Gamma}_1}{\varepsilon - \tilde{\varepsilon}_1 + i\tilde{\Gamma}_1} - \frac{\tilde{\Gamma}_2}{\varepsilon - \tilde{\varepsilon}_2 + i\tilde{\Gamma}_2}. \tag{7}$$

In order to properly evaluate the integral given by Eq. (2), the transmission amplitude must be expressed as a function of k. With the help of $\varepsilon = \hbar^2k^2/2m$ we obtain

$$t(k) = \frac{\chi_1}{k^2 - \epsilon_1 + i\chi_1} - \frac{\chi_2}{k^2 - \epsilon_2 + i\chi_2}, \tag{8}$$

where $\epsilon_n = (2m/\hbar^2)\tilde{\varepsilon}_n$ and $\chi_n = (2m/\hbar^2)\tilde{\Gamma}_n$. We rewrite the above expression by decomposing each of the terms into partial fractions by using the Mittag-Leffler theorem.[18] This results in

$$t(k) = \frac{1}{2}[\zeta_1 f_1(k) - \zeta_2 f_2(k)], \tag{9}$$

where

$$f_n(k) = \frac{1}{k - \kappa_n + i\Upsilon_n} - \frac{1}{k - \kappa_n - i\Upsilon_n} \tag{10}$$

and

$$\zeta_n = \frac{\chi_n}{\kappa_n - i\Upsilon_n}, \tag{11}$$

with

$$\kappa_n = \frac{1}{\sqrt{2}}\left[\left(\epsilon_n^2 + \chi_n^2\right)^{1/2} + \epsilon_n\right]^{1/2}, \tag{12a}$$

$$\Upsilon_n = \frac{1}{\sqrt{2}}\left[\left(\epsilon_n^2 + \chi_n^2\right)^{1/2} - \epsilon_n\right]^{1/2}. \tag{12b}$$

Inserting Eqs. (9)–(12b) into Eq. (2) and following the analytic procedure along the lines of Ref. 15, we obtain the solution of the problem, namely,

$$\psi(x,t) = e^{i(k_0x - \hbar k_0^2 t/2m)}\sum_{n=1}^{2}\tilde{\zeta}_n[M(y_n^-) + M(y_n^+)], \tag{13}$$

where $\tilde{\zeta}_n = (-1)^n i(\sigma\pi/\sqrt{2\pi})^{1/2}\zeta_n$, and

$$M(y_n^\pm) = \frac{1}{2}e^{imX^2/2\hbar T}w(iy_n^\pm) \tag{14}$$

is the Moshinsky function, with

$$y_n^\pm(x,t) = e^{-i\pi/4}\sqrt{\frac{m}{2\hbar T}}\left[\mp X \pm \frac{\hbar Q_n^\pm}{m}T\right], \tag{15}$$

where $Q_n^\pm = -k_0 \mp \kappa_n \pm i\Upsilon_n$, $X = x - x_0 - v_0t$, and $T = t - i\tau$, with $v_0 = \hbar k_0/m$, and $\tau = 2m\sigma^2/\hbar$. With the analytic expression of $\psi(x,t)$ given by Eq. (13) we are ready to calculate the probability density $|\psi(x,t)|^2$ as a function of both position and time at any place on the transmitted side of the system.

III. RESULTS

One of the main features of our model is that we can explore, based on an exact analytical formula [Eq. (13)], a wide range of dynamical features of the probability density $|\psi(x,t)|^2$ from the transient to the stationary regime. In our work we are interested in analyzing the effects of Gaussian wave packet scattering by a double-dot AB interferometer, particularly how

the trapping effects of the molecular states of the system are manifested on the time-dependent features of the scattered wave packet.

A. Effects of the width of the initial wave packet and the incidence energy

An important aspect that cannot be ignored in our dynamical analysis of wave-packet scattering is the relationship of both the energy E_0 and the spectral width of the incident packet with the separation of the molecular states of the AB interferometer. Therefore, we find it natural to define the ratio $r = \Delta k/\Delta k_{2,1}$, where $\Delta k = 1/2\sigma$ is the width of the incident packet in the k space (in the small truncation regime) and $\Delta k_{2,1} \equiv k_2 - k_1$ (with $k_n = \sqrt{2m\tilde{\varepsilon}_n}/\hbar$) is the separation of the molecular states in momentum k space, where the effective mass is given by $m = 0.067\, m_e$, m_e being the electron mass. Since the scattering of the wave packet may be highly sensitive to variations of the incidence energy depending on the value of r, lets us briefly analyze the effects of the incidence energy. Figure 2(a) displays a scattered wave packet that is spectrally wide ($r = 11.6$) for three different incidence energies chosen in the region around the molecular resonances: $E_0 = \varepsilon_0$ (solid line), $E_0 = 0.2\varepsilon_0$ (blue dashed line), and $E_0 = 2\,\varepsilon_0$ (red dotted line). The parameters of the molecule are $\Gamma = 1$ meV, $\varepsilon_0 = 6\Gamma$, and $t_c = \Gamma$, and we use these values throughout the paper, as well as the relation $x_0 = -20\sigma$ (which guarantees the small truncation regime). As is evident from the graphs of Fig. 2(a), the three plots are essentially the same and completely overlap. This occurs because the incident packet is so broad in momentum space that it has k components that can interact with both system's resonances for the three chosen incidence energies. However, this is not the case for smaller values of the ratio r as shown in Fig. 2(b) for $r = 1.4$. This packet is relatively narrow in momentum space, implying that most of its k components are packed in a relatively short interval around k_0. For an incidence energy below ε_0, most of these components are shifted below the system's resonances, so that only a few components of the upper tail of the packet (in k space) have the chance to match those resonances. As a result, the transmission is considerably reduced, as shown in the corresponding curve in Fig. 2(b), for $E_0 = 0.2\varepsilon_0$ (blue dashed line). A similar situation occurs for an incidence energy above ε_0; only components in the lower tail of the incident packet are allowed to transmit through the resonances of the system, while the main bunch of k components are reflected. As a consequence the corresponding transmitted packet is dramatically reduced, as seen in 2(b) when $E_0 = 2\varepsilon_0$ (red dotted line). Only with the choice with $E_0 = \varepsilon_0$ can an important amount of the k components of the incident wave packet be placed into both resonance windows of the system, and hence the transmitted packet, represented by the black solid line in Fig. 2(b), becomes strong and similar in shape to the cases displayed in panel (a).

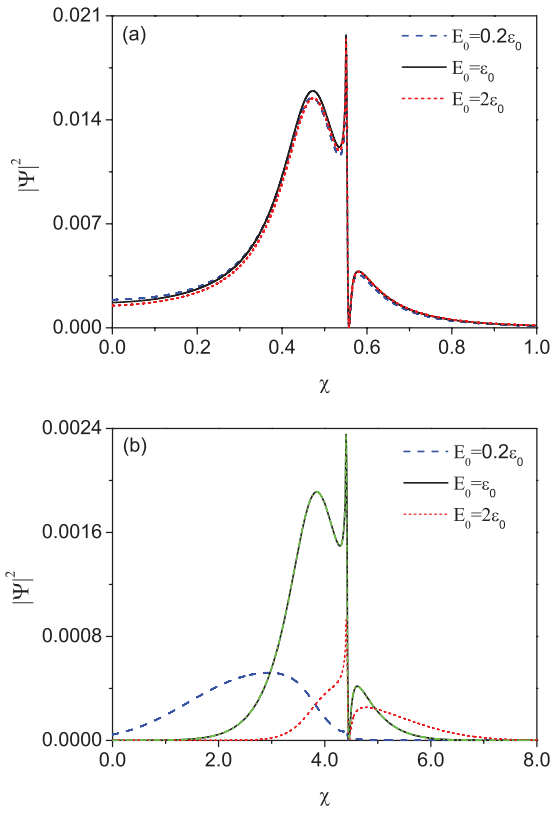

FIG. 2. (Color online) Probability density $|\Psi|^2 = |\psi|^2\sqrt{1+(t/\tau)^2}$ as a function of the distance $\chi = x/(\sigma\sqrt{1+(t/\tau)^2})$ for different values of energy of the incident packet at $t = 5$ ns, with $\phi = \pi/4$, $x_0 = -20\sigma$, for (a) $\sigma = 2.5$ nm ($r = 11.6$) and (b) $\sigma = 20.0$ nm ($r = 1.4$). Just for comparison, the calculation using Eq. (1) integrating numerically over the finite interval $0 \leqslant k \leqslant 0.02$ is included in the case $E = \varepsilon_0$ (dashed-dotted green line). The resulting graph is undistinguishable from the analytical calculation from Eq. (13) (solid line).

In the present study, we are interested in situations where the incident wave packet can interact with both resonances. According to the previous analysis, this is guaranteed when the wave packet is spectrally wide, but for spectrally narrow wave packets the incidence energy should be chosen near both resonances. Therefore, we use $E_0 = \varepsilon_0$ in the rest of the paper since we consider cases with r of the order of unity. We also show in Fig. 2(b) that the numerical integration in Eq. (1) performed over an appropriate finite positive interval gives essentially the same result as the analytical solution.

B. Transient and trapping effects

Since we are interested in the analyzing the transient effects of the scattered wave packet, we conduct our study in the time domain at a selected position in space. Figure 3(a) shows a $|\psi|^2$ vs t graph for a cutoff wave packet with spatial width $\sigma = 2.91$ nm ($x_0 = -58.2$ nm) incident on the AB interferometer. An oscillating transient appears embedded in the wave packet, whose shape and involved frequencies contain relevant information of the internal dynamics occurred in the molecule during the tunneling process. This information "travels" embedded in the transmitted wave packet so that it can be seen outside the system as shown in this figure at the indicated position, and hence may exhibit characteristic features of the molecular spectrum. One such feature that is obvious in Fig. 3(a) is the evolution of the Fano-zero characteristic, whose time of arrival at the position x can actually be analytically calculated from the formal solution [Eq. (13)], using the

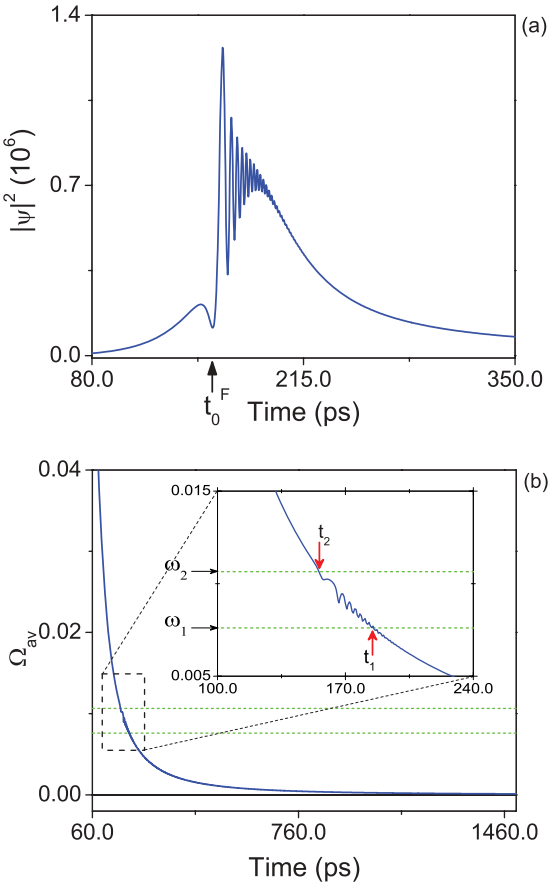

FIG. 3. (Color online) (a) Transient behavior of the probability density as a function of time at a fixed position $x = 3.0 \times 10^4$ nm. The arrow indicates the time t_0^F calculated by Eq. (16). (b) Average frequency Ω_{av} for the same fixed position. The inset shows more detail of the graph in the enclosed area. Here, $\phi = \pi/4$ and $r = 10$.

stationary-phase method.[19] Such expression is given by[20]

$$t_0^F(x) = \frac{x - x_0}{\sqrt{\frac{2}{m}\left[\varepsilon_0 + t_c \sec(\phi/2)\right]}}. \tag{16}$$

The above expression also establishes an explicit relation between the position of the Fano profile in the time domain and the AB phase ϕ, allowing us to easily manipulate its location just by varying the magnetic flux. The position of t_0^F calculated with this formula is indicated with an arrow in Fig. 3(a) and perfectly coincides with the minimum of the characteristic Fano line. Notice that the Fano-zero characteristic is still in formation at this position ($x = 3.0 \times 10^4$ nm) and the characteristic minimum is still different from zero; it reaches the zero value for long-enough distances when the scattered wave packet reaches its final shape.

To explore more closely the internal dynamics in the AB interferometer, we perform a time-frequency analysis, which is a useful tool that relies on the study of the *spectrograms*.[21] The spectrograms correspond to plots of the dominant or average frequency Ω_{av} as a function of time, where $\Omega_{av} = -\mathrm{Im}\left[(\partial\psi/\partial t)/\psi\right]$. The corresponding spectrogram for the wave packet of Fig. 3(a) is shown in Fig. 3(b). As we can see in this case, the dominant frequency is a monotonically decreasing function of time, except in the amplified region shown in the inset, where it exhibits an oscillatory structure in the band defined by the frequencies $\omega_1 = \tilde{\varepsilon}_1/\hbar$ and $\omega_2 = \tilde{\varepsilon}_2/\hbar$. Note also that the crossovers of the spectrogram with the horizontal green dotted lines (corresponding to ω_1 and ω_2) occur at the "times of flight" defined by the classical kinematical relations $t_1 = (x - x_0)/v_1 = 185$ ps and $t_2 = (x - x_0)/v_2 = 156$ ps, respectively, where $v_n \equiv \sqrt{2\tilde{\varepsilon}_n/m}$. The above is a clear evidence that the observed structure on the graph is a signature of the molecular states $\tilde{\varepsilon}_1$ and $\tilde{\varepsilon}_2$ on the transmitted packet.

The wave packet considered in Fig. 3 is spectrally wide in comparison to the separation of the molecular states ($r = 10$) and hence a small percentage of their k components lie in the vicinity of the system's resonances. Let us now consider narrower wave packets in the k space ($\Delta k \lesssim \Delta k_{2,1}$). The reduction of r to a fraction of unity produces dramatic effects as we can see in Fig. 4(a), where we show spectrograms for different values of ϕ (within the interval $0 < \phi < \pi$) for the case $r = 0.3$ (left panel). Notice that the dominant frequency Ω_{av}, instead of being a monotonically decreasing function of time as in Fig. 3, here is retained at the value of ω_2 during a finite time interval (which we call here *retention time*). The chosen variation of ϕ in this sequence of graphs illustrates how this retention time can be further increased, in such a way that the AB interferometer acts as a source of coherent emission with a well-defined frequency. The corresponding DOS curves (computed as in Refs. 3 and 6) are included in the figure (right panel) as a visual aid that allows us to relate the progressive narrowing of the Fano peak with the increase of the retention time. In contrast to the sharp (long-lived) Fano resonance, the broad (short-lived) Breit-Wigner peak is so small and broad in comparison that it can barely be appreciated in the DOS curves (see insets for more detail). If the Fano resonance is not sharp enough, no retention will occur at this position. For example, for $\phi = \pi/2$ (red dashed line) the spectrogram looks quite similar to the case of Fig. 3 (monotonically decreasing). For the sake of comparison, we include this case in the three graphs of Fig. 4(a).

As is well known, when the AB phase is changed to the interval $\pi < \phi < 2\pi$, the roles of the molecular states are interchanged in such a way that $\tilde{\varepsilon}_1$ is now the (narrow) Fano line, and $\tilde{\varepsilon}_2$ is the (broad) Breit-Wigner resonance.[3] Therefore, it is expected that the retention of Ω_{av} will occur at the value of ω_1 instead of ω_2. This is exactly what occurs as we can see in the spectrograms of Fig. 4(b) (left panel), illustrating how this device can work as a frequency selector, switching the frequencies just by properly manipulating ϕ [note also that this switching also occurs automatically in the time scale t_0^F given by Eq. (16)]. As we can also note in Fig. 4(b), the retention time of Ω_{av} at the frequency ω_1 is gradually increased as ϕ tends to 2π (with a concomitant narrowing of the Fano DOS peak as shown in the right panel).

If we continue to reduce the width of the Fano resonance by taking $\phi \to 0$ but finite as in Fig. 4(a), the retention time can be further extended, as shown in the spectrogram for $\phi = \pi/100$ in Fig. 5. However, in the limit $\phi = 0$ this situation is suddenly switched off, as we can see in Fig. 5 where the spectrogram coincides with the case $\phi = \pi/2$. This result shows that the antibonding state, which in this limit has become a localized state,[6] is no longer capable of producing

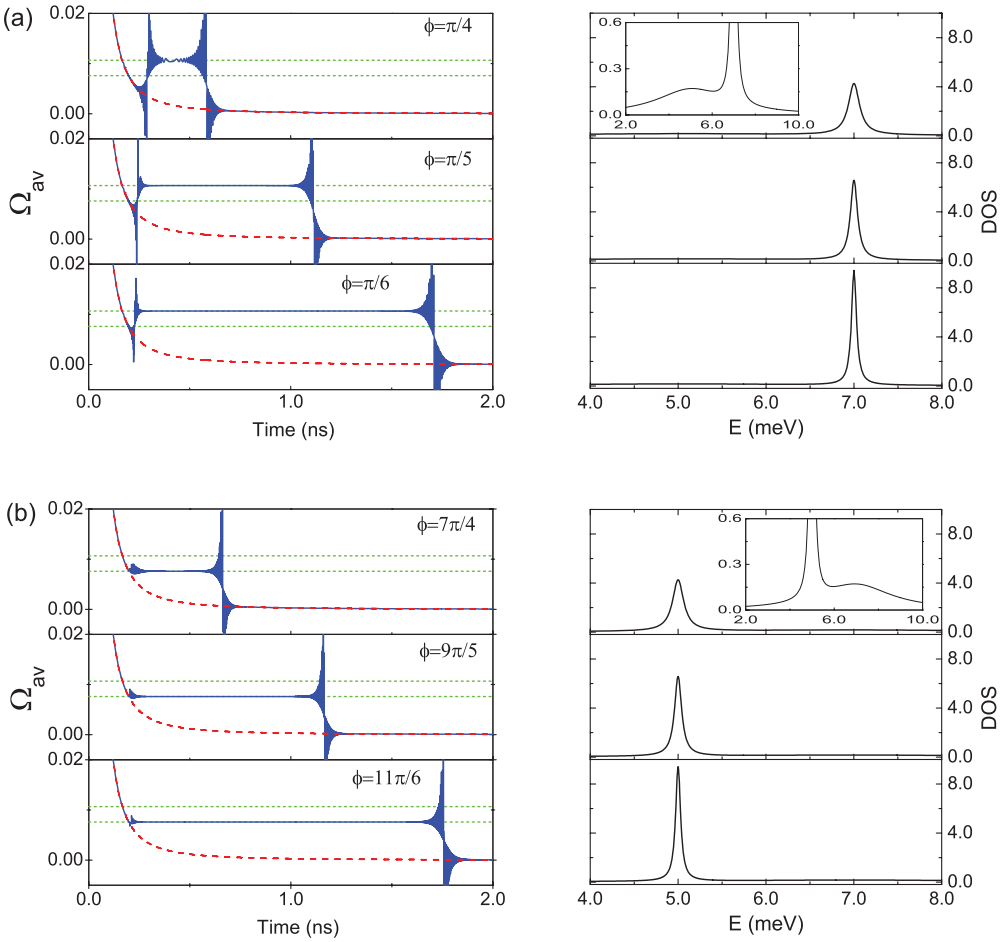

FIG. 4. (Color online) The spectrograms show the trapping effects of the Fano resonance at the fixed position $x = 3.0 \times 10^4$ nm, for different values of ϕ where (a) $\tilde{\varepsilon}_2$ plays the role of the Fano resonance (solid blue lines), and (b) $\tilde{\varepsilon}_1$ plays the role of the Fano resonance (solid blue lines). The cases $\phi = \pi/2$ and $\phi = 3\pi/2$ are included for comparison in (a) and (b), respectively (dashed red lines). The green short-dashed lines represent the same as in Fig. 3(b). The right panels show the corresponding DOS curves. In the insets of cases $\phi = \pi/4$ and $\phi = 7\pi/4$ we include amplifications that allow us to see the Breit-Wigner peaks.

the capture and release effects observed for finite width Fano resonances.

We end this section with a remark concerning the start of the retention periods observed in the spectrograms of Fig. 4. As we can see, in all cases displayed in Fig. 4(b) the retention interval starts roughly at the time t_1, which corresponds to the crossover of the decaying Ω_{av} vs t graph of the packet with the horizontal green short-dashed line sketched at the frequency ω_1 [this time is indicated more clearly with an arrow in the inset of Fig. 3(b)]. In the cases of Fig. 4(a), on the other hand, no retention is observed from the time t_2 onwards. Instead of this, the retention starts a little after t_1 as is evident by simple visual inspection of the spectrograms. This delay is due to the fact that for $0 < \phi < \pi$ the Fano structure travels in the front of the wave packet [as illustrated for example in Fig. 2(a)], arriving at the fixed point x before the main body of the wave packet. Once the Fano structure reaches the fixed point x approximately at the time t_2 (and exactly at the time t_0^F), so does the rest of the packet, and consequently the Fano contribution to the Ω_{av} frequency is "contaminated" by other frequencies during the passage of this bulk by x, producing the observed delay. The oscillatory structures observed in the spectrogram result from the fact that the Fano frequency is competing strongly with these other frequencies of the packet. It is not until the end of the passage of the main body of the packet that the Fano frequency ω_2 begins to dominate.

C. Exponential decay of the Fano resonance

The physical explanation by which the value of Ω_{av} is retained at the Fano frequency for a finite period of time relies on the trapping of wave packet components by the Fano resonance. During the scattering process, the k components of the incident packet with energies around the Fano resonance are temporarily trapped by the interferometer contributing to the formation of a quasistationary state. The trapped components are not released immediately by the molecule; they instead escape from the system obeying the exponential decay law at a rate dictated by the lifetime of the Fano resonance. The delayed components travel embedded in the wave packet arriving at a fixed position as a monochromatic wave. In order to illustrate the above, in Fig. 6 we show a graph of the logarithm of the probability density for the case $\phi = \pi/6$ (solid blue line). As is clearly appreciated, a portion

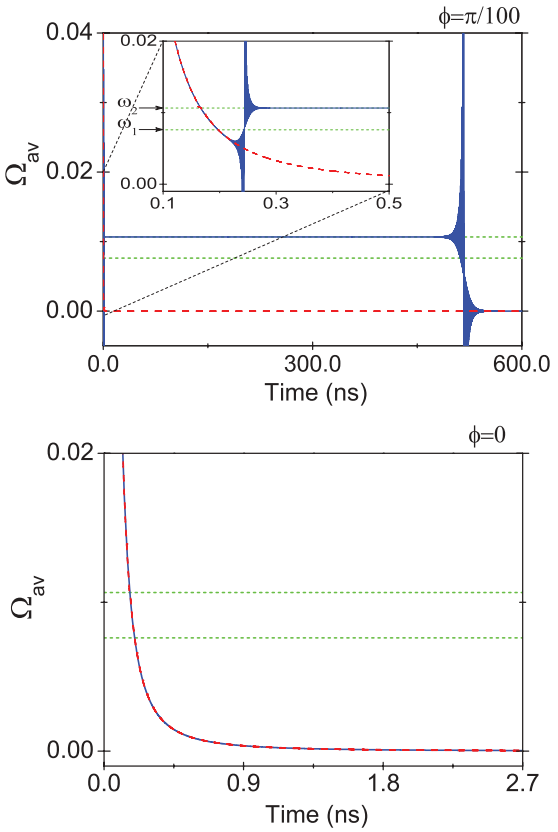

FIG. 5. (Color online) The same as in Fig. 4(a) for a very sharp Fano resonance (top graph) where the inset shows an amplified region at short times, and for the ghost Fano limit (bottom graph). The case $\phi = \pi/2$ is included in both graphs for comparison (dashed red line). Both the blue solid and the red dashed curves are indistinguishable here.

of the $\mathrm{Ln}|\Psi|^2$ vs t graph is a straight line segment that occurs in a time interval that has the same duration as the retention time of Ω_{av} at ω_2 in the corresponding spectrogram of Fig. 4(a) (bottom graph in left panel). Moreover, the slope of this straight segment obtained by numerical inspection is $-103\ \mathrm{ns}^{-1}$, which coincides exactly with the value computed using the width of the Fano resonance of the case $\phi = \pi/6$, that is, $-2\tilde{\Gamma}_2/\hbar$. The case $\phi = \pi/2$ (without retention) is also included for comparison (dashed red line). In contrast to the above case, the corresponding $\mathrm{Ln}|\Psi|^2$ vs t graph does not exhibit exponential decay. Just to help the eye, we also include in Fig. 6 two straight lines with slopes $-103\ \mathrm{ns}^{-1}$ and $-891\ \mathrm{ns}^{-1}$ (green short-dashed lines), calculated from $-2\tilde{\Gamma}_2/\hbar$ using the widths $\tilde{\Gamma}_2$ associated to the cases $\phi = \pi/6$ and $\phi = \pi/2$, respectively. In the former case, the line has the same slope of the straight segment of the corresponding $\mathrm{Ln}|\Psi|^2$ vs t graph, while in the latter case the straight line is so pronounced that it lies well below the tail of the wave packet, and as a consequence, the exponential decay of the Fano resonant state becomes eclipsed by the nonexponential contributions of the wave packet, and the decaying part of the $\mathrm{Ln}|\Psi|^2$ vs t graph is predominantly nonexponential (dashed red line).

In a given fixed position, what determines that the transmitted wave packet exhibits or does not exhibit exponential decay is a proper combination of the values of the parameters

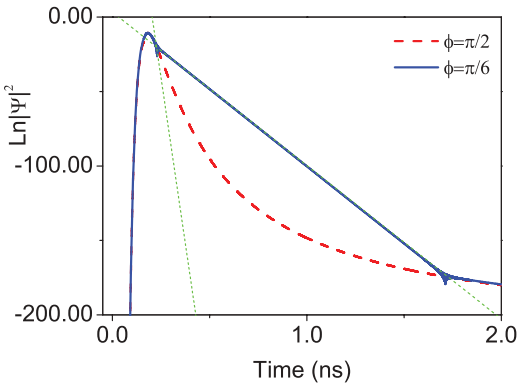

FIG. 6. (Color online) Logarithm of the probability density as a function of time at a fixed position $x = 3.0 \times 10^4$ nm, with $r = 0.3$, for $\phi = \pi/6$ (solid blue line) and $\phi = \pi/2$ (dashed red line). Notice in the case $\phi = \pi/6$ the exponential decay occurring during an interval that coincides with the retention time exhibited in the corresponding spectrogram of Fig. 4(a). On the other hand, the case $\phi = \pi/2$ does not exhibit exponential decay. We also included two straight lines (short-dashed green lines) with slopes $-2\tilde{\Gamma}_2/\hbar$ using the values of $\tilde{\Gamma}_2$ corresponding to $\phi = \pi/6$ and $\phi = \pi/2$.

r and ϕ, which can be varied independently to control the existence and duration of the exponential regime. If we keep r constant (say $r = 0.3$) and let ϕ to take different values (say $\phi = \pi/2, \pi/4, \pi/5, \pi/6$), the width of the Fano resonance is

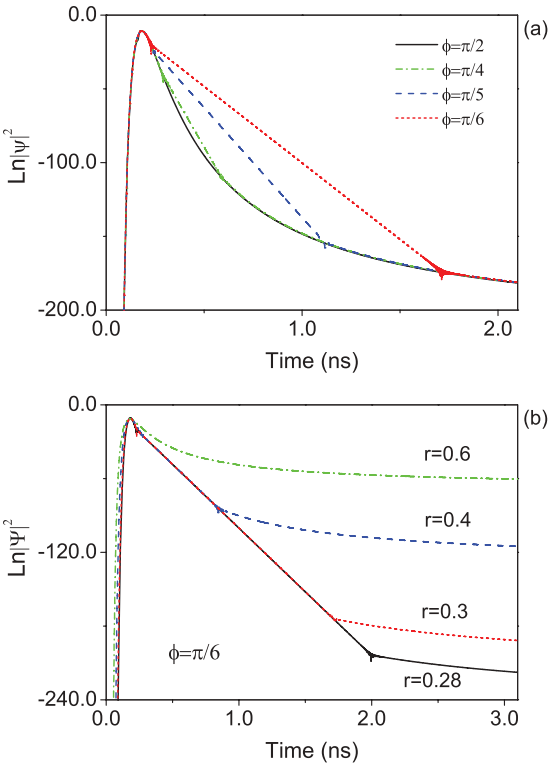

FIG. 7. (Color online) Logarithm of the probability density as a function of time at a fixed position $x = 3.0 \times 10^4$ nm, for (a) $r = 0.3$ and different values of ϕ and (b) $\phi = \pi/6$ and different values of r. The case $\phi = \pi/2$ in (a) does not exhibit exponential decay and it is included for comparison (solid line). The same occurs in (b) for the case $r = 0.6$.

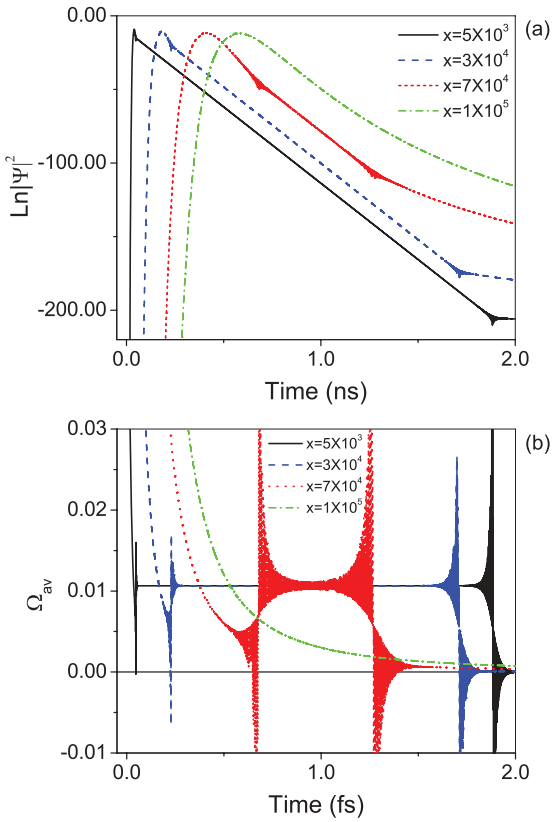

FIG. 8. (Color online) (a) Logarithm of the probability density as a function of time for different positions x (in nm) at $r = 0.3$ and $\phi = \pi/6$. (b) Spectrograms for the cases shown in (a). The different positions are indicated in the graphs in nm. The case $x = 1.0 \times 10^5$ nm does not exhibit exponential decay in (a) and retention in (b).

gradually reduced, increasing in this way the lifetime of the corresponding quasistationary state. As a consequence, the trapped k components of the incident wave packet escape at a slower rate, which is manifested as an increase of the slope $-2\tilde{\Gamma}_2/\hbar$. The above can be appreciated in Fig. 7(a), where the duration of the exponential part of the curve is increased as ϕ goes from $\pi/4$ to $\pi/6$. For $\phi = \pi/2$ the transmitted wave packet does not exhibit exponential decay, since the decay rate of the Fano quasistationary state is faster than the decay rate of the rest of the packet, as a consequence, the slope of the corresponding straight line is so pronounced that the exponential contribution is totally concealed by the rest of the transmitted wave packet, and therefore the nonexponential decay dominates in the whole time domain.

If we now vary r keeping ϕ fixed, the width of the Fano resonance is constant (hence the slope $-2\tilde{\Gamma}_2/\hbar$) and only the nonexponential part of the packet is modified. This is illustrated in Fig. 7(b) for $\phi = \pi/6$ and r taking the values indicated in the graph. For $r = 0.6$ the nonexponential decay rate of the packet is slower than the exponential decay associated to the Fano resonance, and hence there is no exponential regime in this case [similarly as in the case $\phi = \pi/2$ with $r = 0.3$ shown in Fig. 7(a)]. For $r = 0.4$, 0.3, and 0.28 there are finite time intervals where the exponential portion of the $\mathrm{Ln}|\Psi|^2$ vs t graph (straight line) dominates.

In order to complete our analysis, we now explore the effects of variations on the position x on both the duration of the exponential regime and the retention time in the corresponding spectrograms. Figure 8(a) shows the values of $\mathrm{Ln}|\Psi|^2$ as a function of time for different positions indicated in the graph (with r and ϕ fixed). Since r and ϕ are fixed, the width Δk of the initial packet and the width of the Fano resonance are constant, and hence the effects shown in Fig. 7 do not occur. However, as the transmitted packet propagates it becomes broader, and as a consequence, the exponential regime is gradually suppressed, which is manifested in the $\mathrm{Ln}|\Psi|^2$ vs t graphs of Fig. 8(a) as a dramatic reduction of the length of the straight segment of the graph, until it collapses into a single point where the exponential regime disappears. The case $x = 1.0 \times 10^5$ nm shown in Fig. 8 does not exhibit exponential decay because the transmitted wave packet at this position is so broad that the nonexponential decay rate of its tail dominates over the exponential decay of the Fano quasistationary state.

IV. CONCLUDING REMARKS

In summary, the trapping effects of the molecular states in a double-QD AB interferometer on the transient behavior of scattered Gaussian wave packets has been analyzed by means an exact analytical solution of the problem. We have found that a coherent emission embedded in the transmitted wave packet is produced during a finite time interval as a consequence of the formation and decay of a long-lived quasistationary state at the Fano resonance. This emission is characterized by a dominant frequency that is unequivocally related to the molecular state n that plays the role of the Fano resonance, $\Omega_{av} = \tilde{\varepsilon}_n/\hbar$. The retention time of the dominant frequency at this value can be arbitrarily extended by reducing the width of the Fano resonance through manipulations of the AB phase ϕ. However, in the limit of zero width, the coherent emission is switched off since the long-lived state is totally localized.

ACKNOWLEDGMENTS

R.R. and J.V. acknowledge financial support of Facultad de Ciencias UABC under Grant No. P/PIFI 2011-02MSU0020A-08. M.L.L.de G. acknowledges support from Fondecyt under Grant No. 1080660.

*romo@uabc.edu.mx

[1]Z. Z. Sun, R. Q. Zhang, W. Fan, and X. R. Wang, J. Appl. Phys. **105**, 043706 (2009); Y. Han, W. Gong, H. Wu, and G. Wei, Physica B **404**, 2001 (2009); W. Gong, Y. Han, and G. Wei, J. Phys.: Condens. Matter **21**, 175801 (2009); Z. Y. Zeng, F. Claro, and A. Perez, Phys. Rev. B **65**, 085308 (2002); E. R. Racec and U. Wulf, *ibid.* **64**, 115318 (2001).

[2]Kicheon Kang and Sam Young Cho, J. Phys.: Condens. Matter **16**, 117 (2004).

[3]P. A. Orellana, M. L. Ladrón de Guevara, and F. Claro, Phys. Rev. B **70**, 233315 (2004).
[4]Bing Dong, X. L. Lei, and N. J. M. Horing, Phys. Rev. B **77**, 085309 (2008).
[5]T. Hatano, T. Kubo, Y. Tokura, S. Amaha, S. Teraoka, and S. Tarucha, Phys. Rev. Lett. **106**, 076801 (2011).
[6]M. L. Ladrón de Guevara, F. Claro, and P. A. Orellana, Phys. Rev. B **67**, 195335 (2003).
[7]D. M. Kennes and V. Meden, Phys. Rev. B **85**, 245101 (2012); H. Pan, L. N. Zhao, and L. Rong, Physica E **40**, 2988 (2008); H. Pan, S. Q. Duan, W. D. Chu, and W. Zhang, Phys. Lett. A **372**, 3292 (2008); B. Dong, I. Djuric, H. L. Cui, and X. L. Lei, J. Phys.: Condens. Matter **16**, 4303 (2004).
[8]E. Taranko, M. Wiertely, and R. Taranko, J. Appl. Phys. **111**, 023711 (2012); Z. T. Jiang, J. Yang, Y. Wang, X. F. Wei, and Q. Z. Han, J. Phys.: Condens. Matter **20**, 445216 (2008); R. Taranko and P. Parafiniuk, Physica E **40**, 2765 (2008); P. Parafiniuk and R. Taranko, *ibid*. **40**, 3078 (2008).
[9]A. Yacoby, M. Heiblum, D. Mahalu, and Hadas Shtrikman, Phys. Rev. Lett. **74**, 4047 (1995).
[10]R. Schuster, E. Buks, M. Heiblum, D. Mahalu, V. Umanski, and Hadas Shtrikman, Nature (London) **385**, 417 (1997).
[11]Kensuke Kobayashi, Hisashi Aikawa, Shingo Katsumoto, and Yasuhiro Iye, Phys. Rev. Lett. **88**, 256806 (2002); Phys. Rev. B **68**, 235304 (2003).
[12]A. W. Holleitner, C. R. Decker, H. Qin, K. Eberl, and R. H. Blick, Phys. Rev. Lett. **87**, 256802 (2001); A. W. Holleitner, R. H. Blick, A. K. Hüttel, K. Eberl, and J. P. Kotthaus, Science **297**, 70 (2002); S. Gustavsson, R. Leturcq, M. Studer, T. Ihn, K. Ensslin, D. C. Driscoll, and A. C. Gossard, Nano Lett. **8**, 2547 (2008).
[13]U. Wulf and V. V. Skalozub, Phys. Rev. B **72**, 165331 (2005); U. Wulf, V. Skalozub, and A. Zakharov, *ibid*. **77**, 045318 (2008).
[14]A. V. Malyshev, P. A. Orellana, and F. Domínguez-Adame, Phys. Rev. B **74**, 033308 (2006).
[15]J. Villavicencio, R. Romo, and E. Cruz, Phys. Rev. A **75**, 012111 (2007).
[16]M. Abramowitz and I. A. Stegun, *Handbook of Mathematical Functions* (Dover, New York, 1964), p. 297.
[17]T.-S. Kim and S. Hershfield, Phys. Rev. B **67**, 235330 (2003).
[18]M. J. Ablowitz and A. S. Fokas, *Complex Variables: Introduction and Applications*, 2nd ed. (Cambridge University Press, Cambridge, 2003), p. 166.
[19]N. Bleistein and R. A. Handelsman, *Asymptotic Expansions of Integrals* (Dover, New York, 1986), p. 219; E. Erdélyi, *Asymptotic Expansions* (Dover, New York, 1956), p. 51.
[20]R. Romo, J. Villavicencio, and M. L. Ladrón de Guevara (unpublished).
[21]L. Cohen, *Time-Frequency Analysis* (Prentice Hall PTR, Upper Saddle River, NJ, 1994).